

JGR Space Physics

RESEARCH ARTICLE

10.1029/2023JA031792

Key Points:

- We studied whistler mode waves inside the mirror mode structures in the magnetosphere using ~ 3 years of MMS satellite data
- Whistler mode waves are frequently observed inside the mirror mode structures which preferentially occur in the dusk sector
- Both theoretical analysis and observations suggest that whistler mode waves are locally excited in the mirror mode structures

Correspondence to:

X. Gao and Q. Lu,
gaoxl@mail.ustc.edu.cn;
qmlu@ustc.edu.cn

Citation:

Chen, R., Gao, X., Lu, Q., Tsurutani, B. T., Miyoshi, Y., Zhou, X., et al. (2023). Observation of whistler mode waves inside mirror mode structures in the Earth's outer magnetosphere. *Journal of Geophysical Research: Space Physics*, 128, e2023JA031792. <https://doi.org/10.1029/2023JA031792>

Received 18 JUN 2023

Accepted 11 OCT 2023

Observation of Whistler Mode Waves Inside Mirror Mode Structures in the Earth's Outer Magnetosphere

Rui Chen^{1,2,3} , Xinliang Gao^{1,3} , Quanming Lu^{1,3} , Bruce T. Tsurutani⁵ , Yoshizumi Miyoshi² , Xuan Zhou^{1,3} , Yangguang Ke^{1,3} , Huayue Chen⁴ , and Jiuqi Ma^{1,3} 

¹CAS Key Lab of Geospace Environment, School of Earth and Space Sciences, University of Science and Technology of China, Hefei, China, ²Institute for Space-Earth Environmental Research, Nagoya University, Nagoya, Japan, ³CAS Center for Excellence in Comparative Planetology, Hefei, China, ⁴Department of Physics, Auburn University, Auburn, AL, USA, ⁵Retired, Pasadena, CA, USA

Abstract Whistler mode waves are commonly observed inside mirror mode structures (MM-Ss) in the magnetosheath. Although MM-Ss have also been detected in the magnetosphere, there is no statistical study investigating the properties of whistler mode waves inside MM-Ss. Using Magnetospheric Multiscale (MMS) satellites, our present study identifies and statistically analyzes whistler mode waves detected inside MM-Ss in the Earth's magnetosphere. Both the observational evidence (bidirectional propagation) and theoretical analyses suggest that whistler mode waves are excited in the low-magnetic-field regions of MM-Ss. Statistical results indicate that whistler mode waves are frequently observed inside the MM-Ss in the dusk sector. Most of these waves (>70%) are in the frequency range of 0.1–0.4 f_{ce} and have amplitudes less than ~ 50 pT. Moreover, most of them are observed to propagate in the direction both parallel and antiparallel to the background magnetic field, and their wave normal angles are typically less than $\sim 40^\circ$. Our study analyzes the properties and generation of whistler mode waves inside MM-Ss and reveals that MM-Ss are a possible source region in the Earth's magnetosphere. Therefore, our study provides new insight into the properties of whistler mode waves inside MM-Ss which are pervasive in space plasmas.

1. Introduction

Whistler mode waves are commonly observed in space plasmas (Burtis & Helliwell, 1969; Gao et al., 2014; W. Li et al., 2012; Meredith et al., 2004; Miyoshi et al., 2003; Tsurutani & Smith, 1974, 1977). These waves are right-handed circularly polarized in the frequency range between the lower hybrid frequency (f_{lh}) and the electron cyclotron frequency (f_{ce}). Previous studies have indicated that anisotropic hot electrons can excite whistler mode waves from cyclotron resonant instabilities (Kennel & Petschek, 1966), and the waves are mainly field aligned with small wave normal angles (the angle between wave vector \vec{k} and background magnetic field \vec{B}_0 , Tsurutani & Smith, 1974, 1977; Miyoshi et al., 2007; Gao et al., 2014; Chen et al., 2017; Lu et al., 2019). Moreover, whistler mode waves can be excited by the Landau resonance with electron beams moving along the background magnetic field, and the waves are quite oblique with wave normal angles larger than $\sim 60^\circ$ (Artemyev et al., 2016; W. Li et al., 2016; Mourenas et al., 2015). In addition, whistler mode waves can also be excited by the electron temperature gradient (Jovanovic & Simic, 2004).

Whistler mode waves are widely observed in the magnetosheath, known as lion roars (Baumjohann et al., 1999; Smith & Tsurutani, 1976; Thorne & Tsurutani, 1981; Tsurutani et al., 1982; Zhang et al., 1998). They are commonly detected inside mirror mode structures (MM-Ss) which are presented as quasiperiodic magnetic oscillations. Tsurutani et al. (1982) showed a strong correlation between the occurrence of lion roars and MM-Ss. Zhang et al. (1998) showed that approximately 30% of lion roars are associated with MM-Ss. Most of these waves are quasi-parallel with wave normal angles less than $\sim 10^\circ$ (Smith & Tsurutani, 1976; Zhang et al., 1998). Recently, MM-Ss have also been detected in the magnetosphere, and they are considered to be excited by anisotropic ions in high β plasmas (L. Li et al., 2023; Rae et al., 2007; Soto-Chavez et al., 2019). L. Li et al. (2023) presented an unusual whistler wave event inside MM-Ss, where the lower-band and upper-band whistler mode waves are observed near the high- and low-magnetic-field regions of MM-Ss, respectively. Their different locations can be explained by nonlinear theory, in which the field configuration of MM-Ss and the modulated electron distributions modify the threshold amplitude of nonlinear wave growth (L. Li et al., 2023). At present, there is no statistical study investigating the properties of whistler mode waves inside MM-Ss in the magnetosphere.

In this paper, using the Magnetospheric Multiscale (MMS) observation data, we identify and statistically analyze whistler mode waves detected inside MM-Ss in the Earth's magnetosphere. A case study reveals that whistler mode waves can be excited through the anisotropic electrons inside the MM-Ss, which is also supported by a linear instability analysis. Statistical results based on the fast/survey-mode data indicate that whistler mode waves are commonly observed inside the MM-Ss, and we further investigate the wave properties (such as wave amplitude, frequency, normal angle, and propagation direction) based on the burst-mode data.

2. Data Sources

The Magnetospheric Multiscale (MMS) mission consists of four identical satellites, and each satellite carries a number of plasma and field instruments to measure plasma distributions and electromagnetic fields (Burch et al., 2016; Fuselier et al., 2016). In this study, the background magnetic field with a resolution of 8 or 16 samples/s (survey mode) is measured by the Fluxgate Magnetometer (FGM, Russell et al., 2016). The burst-mode magnetic and electric waveform data (8,192 samples/s) are provided by the search coil magnetometer (SCM, Le Contel et al., 2016) and spin-plane double probes (SDP, Lindqvist et al., 2016), respectively. For each burst waveform data, a 1024-point fast Fourier transform (FFT) with a 512-point moving window is applied to analyze both magnetic and electric fields. Therefore, the obtained dynamic spectrogram has a temporal resolution of ~ 0.0625 s. In addition, the wave electric and magnetic power spectra with a cadence of 2 s (fast-mode) are provided by the Digital Signal Processor (DSP, Le Contel et al., 2016; Lindqvist et al., 2016). The plasma data are obtained from the Fast Plasma Instrument (FPI, Pollock et al., 2016), which also measures the velocity-space distribution of electrons and ions from 10 eV to 30 keV.

3. Case Study

Figure 1 shows a typical whistler mode wave event inside mirror mode structures (MM-Ss) during 21:20–22:20 UT on 10 October 2016. The MMS-3 satellite was at $L = \sim 11.8$, MLAT = $\sim 11.0^\circ$, and MLT = ~ 17.7 hr. Here, the value of L is calculated based on the dipole field model. Figure 1a presents the frequency-time spectrum of the magnetic field. The magnetic signatures at $\sim 0.1 f_{ce}$ are whistler mode waves correlated with low-magnetic-field regions (Figure 1c). Figure 1b shows that their amplitudes can reach ~ 0.1 nT, comparable to that of chorus waves in the inner magnetosphere. During this time interval, the magnetic oscillations (Figure 1c) are identified as MM-Ss due to the quasiperiodic oscillating magnetic fields with small angular changes across the structures (i.e., the field angles θ and φ have little change in Figure 1d) and the nearly constant total pressure (Figure 1f). These features have been used to identify mirror mode structures (Tsurutani et al., 1982, 2011). During the time, the perpendicular and parallel temperatures of the ions and plasma β were investigated (not shown). There is a $T_{i,\perp}/T_{i,\parallel}$ ion anisotropy, and the averaged plasma β is quite high (i.e., ~ 5). Then, the criterion of mirror instability is roughly given by $R = \beta_{i,\perp}(1 - T_{i,\perp}/T_{i,\parallel}) + 1$ ($\beta_{i,\perp} = \frac{n_i k_B T_{i,\perp}}{B_0^2/2\mu_0}$; Hasegawa, 1969). A negative R means that the criterion of the mirror instability is satisfied. In this event, R is slightly negative during the period with higher anisotropy. Therefore, considering the relaxation of anisotropic ions, this plasma condition favors the generation and existence of mirror mode structures.

Simultaneously, the low plasma densities (Figure 1e) and high fluxes of ~ 10 keV electrons (Figure 1i) indicate that these MM-Ss and whistler mode waves should be inside the magnetosphere. The electron $\beta_e (\frac{n_e k_B T_e}{B_0^2/2\mu_0})$ in Figure 1g is always less than 0.5 in the high-magnetic-field regions but increases to $>\sim 1$ in the low-magnetic-field regions (Figure 1g). In contrast, the cyclotron resonance energy E_c is high (~ 20 keV for $0.1 f_{ce}$) in the high-magnetic-field regions but much lower (~ 5 keV) in the low-magnetic-field regions (Figure 1h). Here, the cyclotron resonance energy is estimated under the first-order cyclotron resonance based on the cold plasma dispersion relation (W. Li et al., 2011). In general, these whistler mode waves are detected with low resonance energies in the low-magnetic-field regions of MM-Ss. There is an anticorrelation between the magnetic field intensity and the plasma density. Mirror modes are total (plasma plus magnetic field) pressure balance structures both in the high and low magnetic field regions (Tsurutani et al., 1982). Both the low magnetic field intensity and high plasma density result in a low resonance energy. Considering the typical electron spectrum, there are more electrons at lower energies and therefore more free energy for wave generation (e.g., W. Li et al., 2011).

To investigate the generation of whistler mode waves inside the MM-Ss, we perform linear theoretical analysis using the method in W. Li et al. (2011). The linear growth rates of parallel-propagating whistler mode waves can be calculated by the formula,

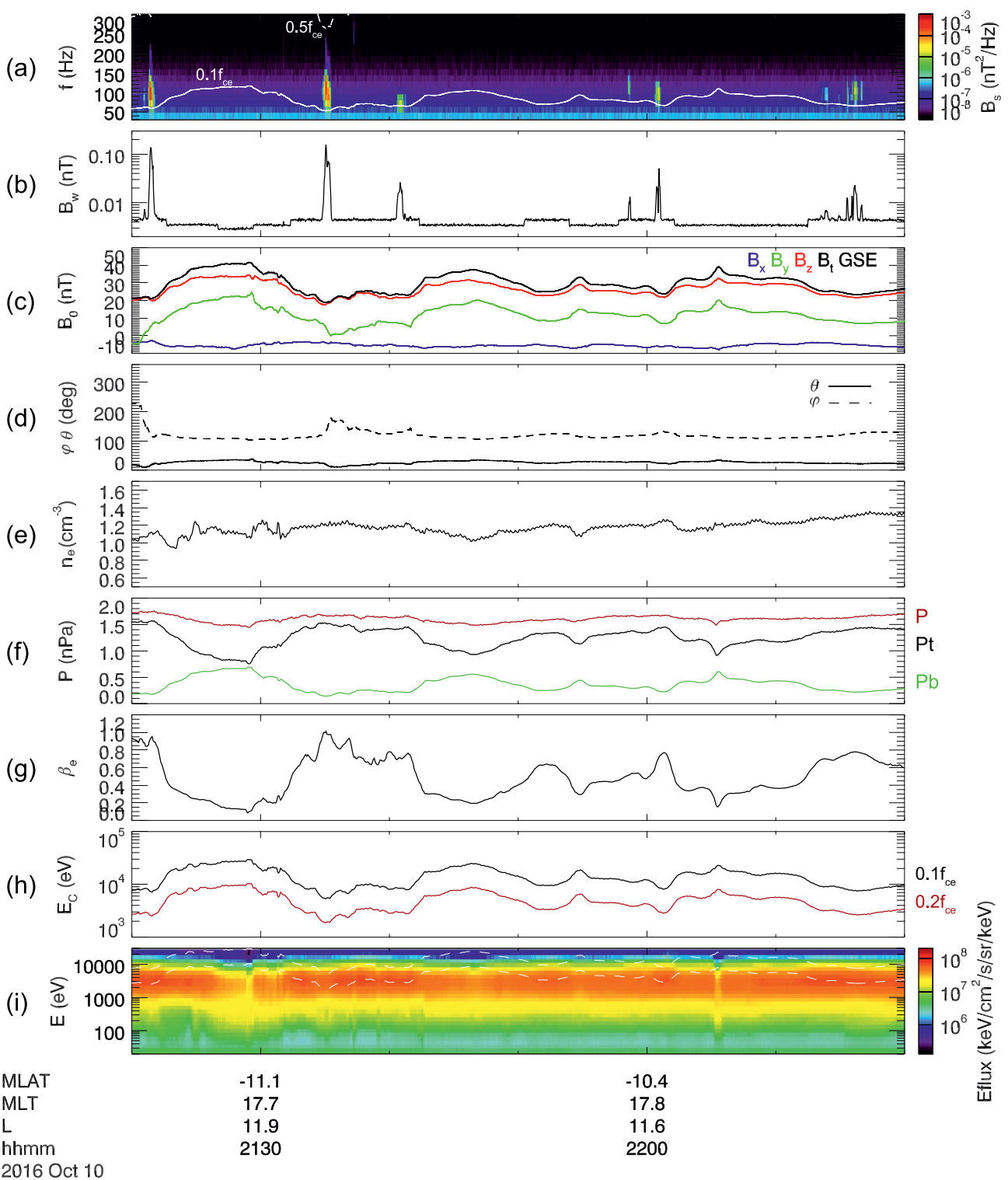


Figure 1. (a) The frequency-time power spectrum of the magnetic field, (b) the wave amplitude integrated between $0.05 f_{ce}$ and $0.8 f_{ce}$ (f_{ce} is the local electron cyclotron frequency), (c) background magnetic field in the GSE coordinate and its sum, (d) two field angles (θ and φ) of the magnetic field, (e) electron number density, (f) total pressure P , thermal pressure P_t and magnetic pressure P_b , (g) electron β_e , (h) the cyclotron resonance energies for $0.1 f_{ce}$ and $0.2 f_{ce}$, and (i) electron differential energy fluxes. In panel d, θ is the angle between the magnetic field vector and z-axis, and φ is the angle between the projection (in the x-y plane) and x-axis. The white lines in panel i represent the resonance energies for $0.1 f_{ce}$ and $0.2 f_{ce}$.

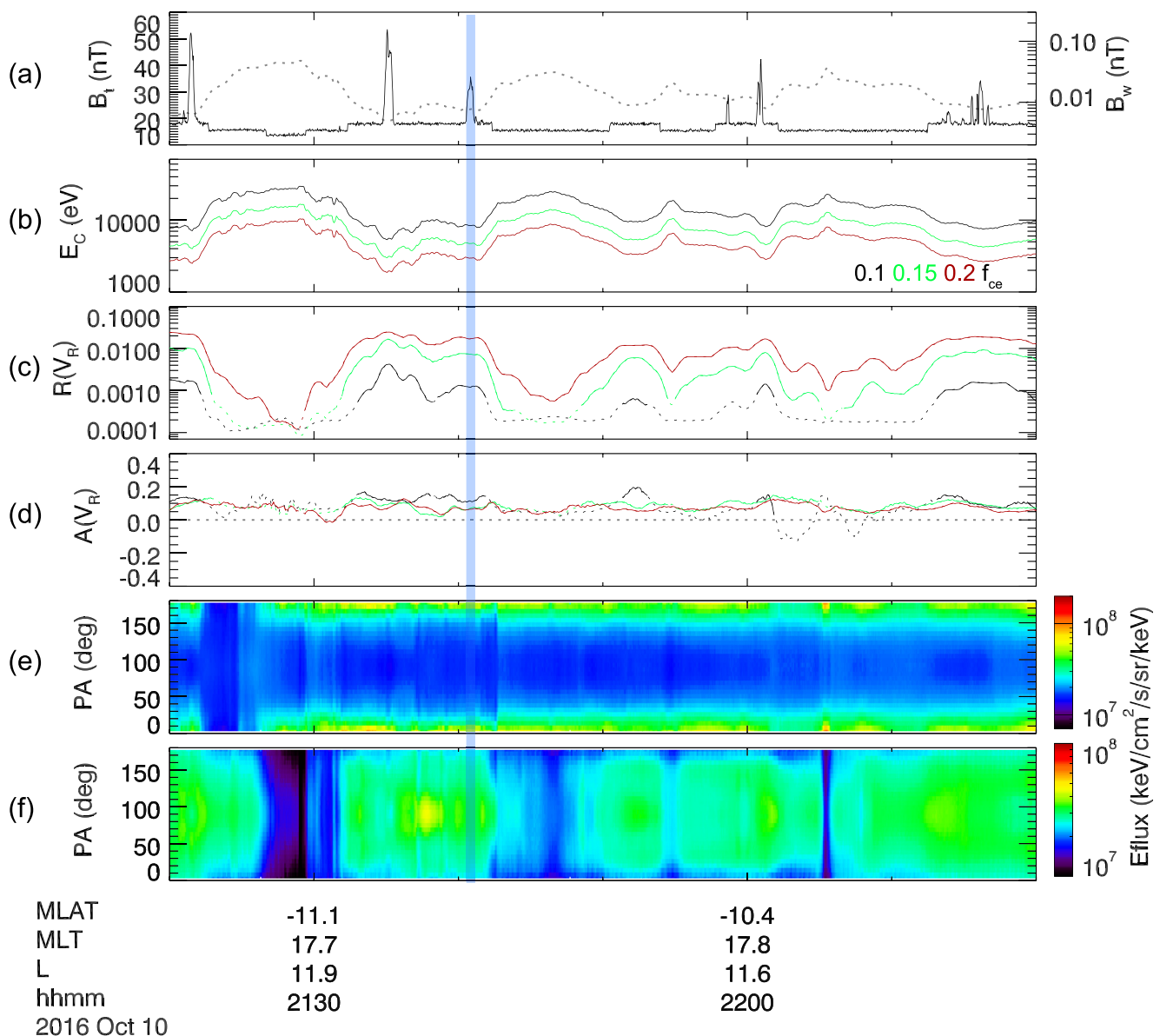


Figure 2. (a) The wave magnetic amplitude and the intensities of the background magnetic field, (b) the cyclotron resonance energies for 0.1, 0.15, and 0.2 f_{ce} , (c) parameter $R(V_R)$, (d) parameter $A(V_R)$, and pitch angle distributions for energy ranges (e) 0.2–2.0 keV and (f) 2.0–30 keV. When the resonance energy is larger than 10 keV, the calculated $R(V_R)$ and $A(V_R)$ are marked by dashed lines.

$$\gamma = \pi |\Omega_{ce}| \cdot R(V_R) \cdot [A(V_R) - A_c], \quad (1)$$

where Ω_{ce} is the electron cyclotron angular frequency, V_R is the parallel velocity of electrons satisfying the first-order cyclotron resonance condition, and A_c is the critical anisotropy which is equal to $1/(\|\Omega_{ce}\|/\omega - 1)$. ω is the wave angular frequency. $A(V_R)$ is the electron anisotropy for a fixed resonance velocity, and $R(V_R)$ roughly represents the ratio of resonant electrons to total electrons.

Figure 2a presents the wave amplitude (solid line) and the intensity of the background magnetic field (dashed line), and Figure 2b shows the cyclotron resonance energies for three typical frequencies (0.1, 0.15, and 0.2 f_{ce}). The resonance energies are in the range of ~2–10 keV for waves with 0.1–0.2 f_{ce} in the low-magnetic-field regions. Based on the electron pitch angle distributions (Figures 2e and 2f) measured by the FPI instrument, the values of $R(V_R)$ and $A(V_R)$ are given in Figures 2c and 2d, respectively. Whistler mode waves are always observed with large values of $R(V_R)$ and positive $A(V_R)$. As shown in Figures 2d and 2f, the positive $A(V_R)$ generally

corresponds to that the electron pitch angle distribution peaking at approximately 90°. Therefore, it is expected that these waves can be generated by the anisotropic electrons, and we investigate a whistler case (marked by the shaded region in Figure 2) in the following section.

Figure 3 shows a whistler case observed inside the MM-S using the burst-mode waveform data. Whistler mode waves satisfying the following criteria are retained: (a) polarization ratio >0.8, (b) ellipticity >0.6, and (c) magnetic field power spectral density >10⁻⁸ nT²/Hz. We also have checked and verified that the noise level is always less than 5 pT (for both the fast and burst data). Figures 3a and 3b present the spectra of the wave magnetic field and electric field, showing that the wave frequencies are at ~0.1 f_{ce} . The wave normal angles presented in Figure 3c remain small values (<~10°). Here, Pf flag indicates the wave propagation direction: “+1” indicates propagating toward the polar region, and “-1” indicates propagating toward the equator region. The mixture of positive and negative values (Figure 3d) suggests the bidirectional propagation of these waves. These results indicate that the observed whistler mode waves are detected in the source region. Figures 3e–3g present the integral values of the wave amplitude, normal angle, and Pf value, which are used to perform the statistical analysis in Figure 6. For each time unit (0.0625 s), the wave amplitude is integrated between 0.05 f_{ce} and 0.8 f_{ce} . The integral θ_{bk} (Figure 3f) and the integral Pf (Figure 3g) are the power-weighted averages of the wave normal angle and Pf value between 0.05 f_{ce} and 0.8 f_{ce} . Utilizing the BO dispersion solver (Xie, 2019), we further calculate the dispersion relation and linear growth rate to verify the generation of whistler mode waves inside the MM-S. Figure 4a shows the simultaneously measured electron phase space density as a function of energy. The electron distribution is obtained by averaging the measurements of FPI from 21:40:40 UT to 21:40:50 UT. Then, the measured electron distribution is fitted by a sum of drifting bi-Maxwellian components as $f = \sum_j f_j, j = 1-6$,

$$f_j = n_{e,j} \sqrt{\frac{m}{2\pi T_{e,\parallel j}}} \frac{m}{2\pi T_{e,\perp j}} \exp\left(-\frac{m(v_{e,\parallel} - v_{bj})^2}{2T_{e,\parallel j}} - \frac{mv_{e,\perp}^2}{2T_{e,\perp j}}\right), \quad (2)$$

where $v_{e,\parallel}$ and $v_{e,\perp}$ are the electron parallel and perpendicular velocities, respectively. $T_{e,\parallel j}$ and $T_{e,\perp j}$ are the parallel and perpendicular temperatures of component j , respectively. The number density of each component is represented by $n_{e,j}$. All of the fitting parameters are presented in Table 1. Figure 4b shows the calculated dispersion relation and linear growth rate, and the wave frequency with the peak linear growth rate is approximately 0.096 f_{ce} , which is consistent with the observations. The electron distribution used to calculate the linear growth rate should be measured after the relaxation of those electrons, and therefore we can speculate that the growth rate based on the electron distribution before wave excitation is much larger than $\sim 10^{-4}\Omega_{ce}$. Moreover, we have estimated the linear growth rate using Equation 1, and the value of the growth rate ($\sim 10^{-4}\Omega_{ce}$, for $f = 0.1 f_{ce}$) is close to the result of the dispersion solver. Although the calculated $A(V_R)$ for 0.15 or 0.2 f_{ce} may be insufficient to produce positive growth rates, it is nevertheless close to the value of critical anisotropy A_c . As a result, both the growth rates calculated by Equation 1 and the dispersion solver indicate that whistler mode waves can be excited in the mirror mode structures.

4. Statistical Results

Using more than 3 years (2015.09–2018.12) of MMS-3 fast/survey-mode data, the distributions of MM-Ss and whistler mode waves in the magnetosphere are shown in Figure 5. Here, the time interval with an electron temperature larger than 100 eV and a plasma density less than 5 cm⁻³ is identified to be located inside the magnetosphere. The L-MLT (Figure 5a) and |MLAT|L (Figure 5d) distributions of spacecraft operating time show that there are enough samples to perform a reliable statistical analysis. Referring to the selection criteria for the MM-Ss in the magnetosheath (Dimmock et al., 2015), we apply a one-hour time window for searching MM-Ss in the magnetosphere and then check each event visually. The distributions of the occurrence rate of MM-Ss in the L-MLT and |MLAT|L planes are presented in Figures 5b and 5e, respectively. Mirror mode structures are mainly observed in the dusk sector (MLT = ~15–19 hr) and occasionally observed in the dawn sector (MLT = ~4–8 hr) near the magnetopause (L = 10–14, Figure 5b). They are distributed over a wide range of latitudes from the equatorial regions to mid-latitudes and peak at |MLAT| = ~10–25° (Figure 5e). Figures 5c and 5f present the distributions of whistler mode waves inside MM-Ss. Overall, whistler mode waves appear during ~10% of the time period that MM-Ss are observed.

Figures 3e–3g present an example of the burst mode data. Here each time unit (0.0625 s) is considered one record and there are 56,503 records (only retaining the record with an amplitude larger than 5 pT). Using the burst-mode

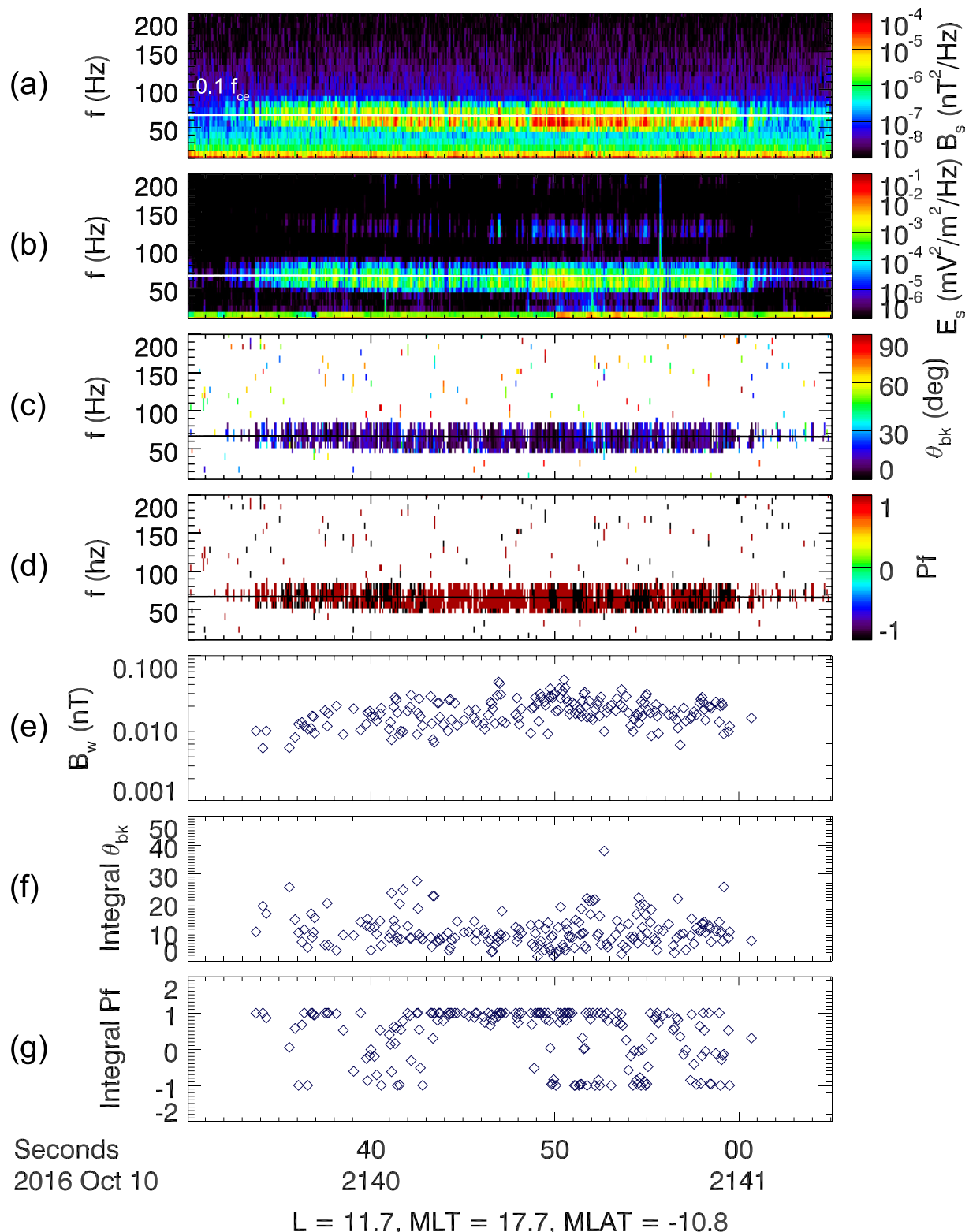


Figure 3. The frequency-time spectra of the (a) wave magnetic field, (b) wave electric field, (c) wave normal angle, and (d) Pf flag, and the integral value of the (e) wave amplitude, (f) wave normal angle, and (g) Pf value for each time unit. Here, Pf indicates the wave propagation direction: “+1” indicates propagating toward the polar region, and “−1” indicates propagating toward the equator region.

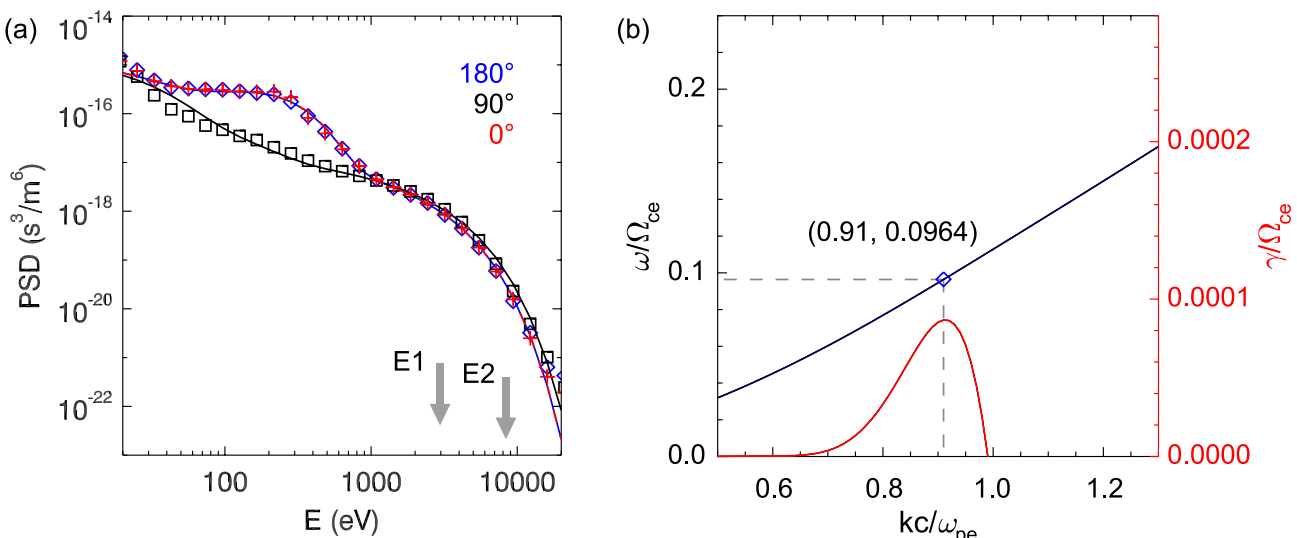


Figure 4. (a) Electron phase space densities and their fitted curves in three directions as a function of energy, (b) dispersion relation and linear growth rate calculated by the BO model. In panel a, observational measurements are represented by symbols, and the fitting curves are represented by lines. Here, red, black, and blue colors represent parallel, perpendicular, and antiparallel directions, respectively. E1 and E2 represent the minimum cyclotron resonance energies for $0.2 f_{ce}$ and $0.1 f_{ce}$, respectively.

data, Figures 6a and 6b present the distributions of wave amplitude and normalized frequency, respectively. Whistler mode waves inside MM-Ss typically have a wave amplitude less than 0.05 nT, with a frequency range of 0.1–0.4 f_{ce} . Figure 6c shows that nearly all of these waves ($\sim 90\%$) have small wave normal angles ($< 40^\circ$). To determine whether an event is located in the source region, a 5-s interval is considered as one event and the integral Pf is also calculated first for each time unit (same as Figure 3). Then, the identification criteria are set as follows: if the number of data points with $|Pf| < 0.5$ ($\#(|Pf| < 0.5)$) is larger than 10% of the total data points ($\#(\text{all})$), or $\#(Pf > 0)/\#(\text{all})$ is in the range 0.1–0.9, this 5-s event is considered to be in the source region. Then, we find that 43.6% of events are observed in the source region. Moreover, we also apply much stricter criteria, and there are still more than 20% of events in the source region (Table 2). Those events that are not identified to be in the source region may propagate either from the magnetic equator or the adjacent mirror mode structures.

Considering the design of the MMS, the burst-mode data are only recorded in the region of particular interest. Therefore, the event number of burst-mode (56,503 records with a sampling period of 0.0625 s determined by the FFT window) is much smaller than that of fast-mode (10.8 hr in total). Although the spatial distribution based on the burst-mode data may have a limitation, the obtained wave properties should remain reliable as shown in Figure 6 and Table 2.

5. Summary and Discussion

In this study, we analyze the properties and generation of whistler mode waves inside the MM-Ss in the Earth's outer magnetosphere, and reveal that the MM-Ss are a possible source region of whistler mode waves. The low-magnetic-field region of MM-S leads to the low resonance energy of electrons for whistler mode waves, and therefore such conditions can lead to electron cyclotron instability to generate significant whistler mode waves. A case study based on the burst-mode data provides direct evidence that whistler mode waves can be excited inside MM-Ss, which is further verified by linear instability analysis. The statistical results using the fast/survey-mode data show that MM-Ss are commonly observed in the dusk sector near the magnetopause ($L = \sim 10\text{--}14$), and whistler mode waves are frequently observed inside the MM-Ss frequently. Based on the burst-mode data, we further find that most of these waves have amplitudes less than ~ 50 pT with

Table 1
The Fitting Parameters for the Electron Distribution in Figure 4a

$B_0 = 23.6$ nT			
	n_e (cm^{-3})	$T_{e,\parallel}$ (eV)	$T_{e,\perp}$ (eV)
#1	0.15	20	20
#2	0.02	100	100
#3	0.10	640	600
#4	0.50	1,600	1,800
#5	0.20	64	80
#6	0.20	64	80

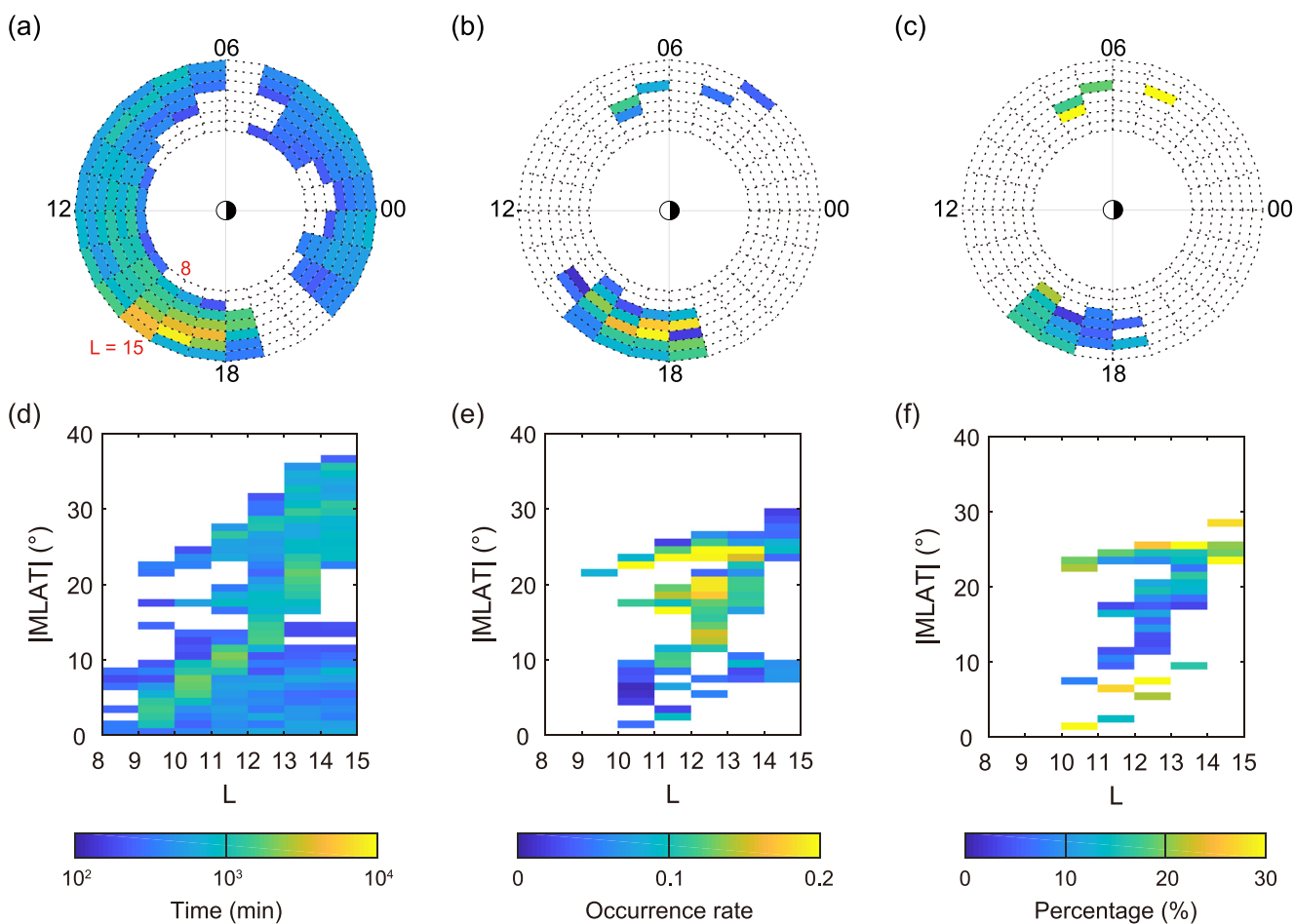


Figure 5. The distributions in the (a) L-MLT plane and (d) |MLAT|-L plane for spacecraft operating time in the magnetosphere (the bin with operating time less than 3 hr is excluded), (b and e) the occurrence rate of MM-S (it is the ratio of observation time of MM-S to spacecraft operating time, and the bin with observation time less than 10 min is excluded), and (c and f) the percentage of whistler mode waves inside MM-S (it is the ratio of the observation time of whistler mode waves to that of MM-S, and the bin with an observation time of whistler waves less than 3 min is excluded).

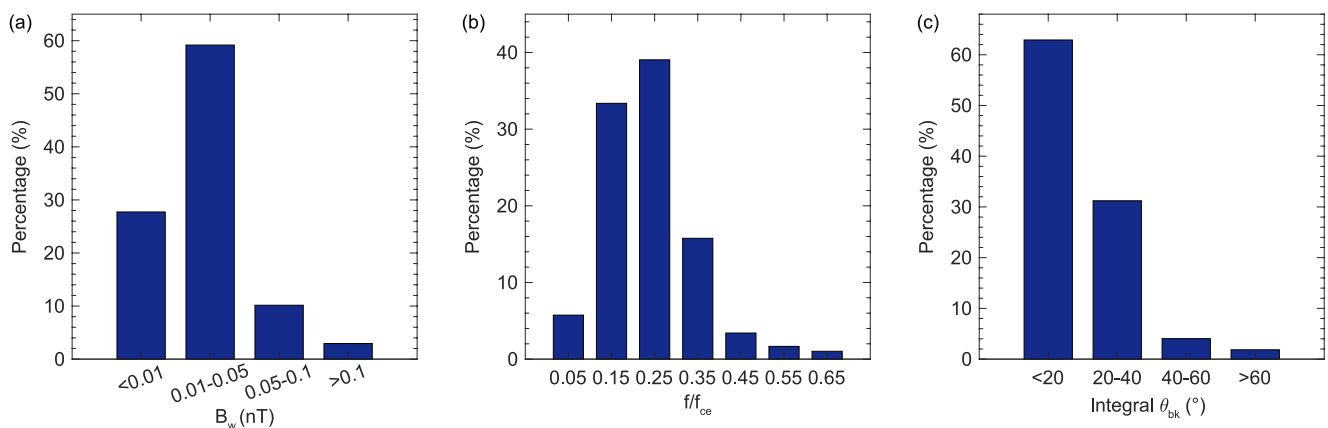


Figure 6. The distributions of (a) wave amplitude, (b) power-weighted wave frequency, and (c) integral wave normal angle based on high-resolution waveform data.

Table 2
Percentage of Wave Events in the Source Region

Criterion	Percentage
$\#(\text{Pf} < 0.5)/\#(\text{all}) > 0.1 \text{ or } 0.9 > \#(\text{Pf} > 0)/\#(\text{all}) > 0.1$	43.6%
$\#(\text{Pf} < 0.5)/\#(\text{all}) > 0.2 \text{ or } 0.8 > \#(\text{Pf} > 0)/\#(\text{all}) > 0.2$	28.7%
$\#(\text{Pf} < 0.5)/\#(\text{all}) > 0.3 \text{ or } 0.7 > \#(\text{Pf} > 0)/\#(\text{all}) > 0.3$	20.7%

a frequency range of 0.1–0.4 f_{ce} . Moreover, most of them are observed to propagate in the direction both parallel and antiparallel to the background magnetic field, and their wave normal angles are typically less than ~40°.

Whistler mode waves are usually detected in the low-magnetic-field regions of the MM-Ss, where the resonant electron densities are highest (Figure 2c) and the electrons are anisotropic (Figures 2d and 2f). Therefore, the cyclotron resonance with anisotropic electrons is the dominant generation mechanism. Based on the THEMIS observations, W. Li et al. (2011) presented that compressional ULF waves can modulate the excitation of whistler mode

waves by regulating the flux of resonant electrons, which tends to occur in the dawn sector. In this study, we show that whistler mode waves modulated by MM-Ss are typically observed in the dusk sector near the magnetopause ($L = \sim 10\text{--}14$), which can complement previous studies.

Mirror mode structures are generated by anisotropic ions with $T_{i\perp}/T_{i\parallel} > 1$ in high β plasmas (Hasegawa, 1969; Treumann & Baumjohann, 2019). In the statistical result, the MM-Ss are mainly observed in the dusk sector, suggesting that substorm injected protons are the main source of free energy. However, the identification of MM-Ss in the dawn sector indicates that the above hypothesis is not the complete picture. The occurrence of MM-Ss at both dusk and dawn at large L (and little elsewhere) points to another mechanism. Further study is needed to resolve these issues. This is beyond the scope of the present work.

Data Availability Statement

The MMS data used in this study are available from the website <https://spdf.gsfc.nasa.gov/pub/data/mms/>. The MMS data analysis is carried out using the publicly available SPEDAS software (<http://spedas.org>).

Acknowledgments

This research was funded by the NSFC Grants (42322406 and 42230201), National Key Research and Development Program of China (No. 2022YFA1604600), the Strategic Priority Research Program of Chinese Academy of Sciences Grant XDB41000000, and the “USTC Tang Scholar” program. Rui Chen also thanks the China Scholarship Council for the support during his study in Japan. We also acknowledge the entire MMS instrument teams.

References

- Artemyev, A., Agapitov, O., Mourenas, D., Krasnoselskikh, V., Shastun, V., & Mozer, F. (2016). Oblique whistler-mode waves in the Earth's inner magnetosphere: Energy distribution, origins, and role in radiation belt dynamics. *Space Science Reviews*, 200(1–4), 261–355. <https://doi.org/10.1007/s11214-016-0252-5>
- Baumjohann, W., Treumann, R. A., Georgescu, E., Haerendel, G., Fornacon, K.-H., & Auster, U. (1999). Waveform and packet structure of lion roars. *Annales Geophysicae*, 17(12), 1528–1534. <https://doi.org/10.1007/s00585-999-1528-9>
- Burch, J. L., Moore, T. E., Torbert, R. B., & Giles, B. L. (2016). Magnetospheric multiscale overview and science objectives. *Space Science Reviews*, 199(1–4), 5–21. <https://doi.org/10.1007/s11214-015-0164-9>
- Burtis, W. J., & Helliwell, R. A. (1969). Banded chorus-A new type of VLF radiation observed in the magnetosphere by OGO 1 and OGO 3. *Journal of Geophysical Research*, 74(11), 3002–3010. <https://doi.org/10.1029/ja074i011p03002>
- Chen, H., Gao, X., Lu, Q., Ke, Y., & Wang, S. (2017). Lower band cascade of whistler waves excited by anisotropic hot electrons: One-dimensional PIC simulations. *Journal of Geophysical Research: Space Physics*, 122(10), 10448–10457. <https://doi.org/10.1002/2017JA024513>
- Dimmock, A. P., Osmane, A., Pulkkinen, T. I., & Nykyri, K. (2015). A statistical study of the dawn-dusk asymmetry of ion temperature anisotropy and mirror mode occurrence in the terrestrial dayside magnetosheath using THEMIS data. *Journal of Geophysical Research: Space Physics*, 120(7), 5489–5503. <https://doi.org/10.1002/2015JA021192>
- Fuselier, S. A., Lewis, W. S., Schiff, C., Ergun, R., Burch, J. L., Petrinec, S. M., & Trattner, K. J. (2016). Magnetospheric multiscale science mission profile and operations. *Space Science Reviews*, 199(1–4), 77–103. <https://doi.org/10.1007/s11214-014-0087-x>
- Gao, X., Li, W., Thorne, R. M., Bortnik, J., Angelopoulos, V., Lu, Q., et al. (2014). New evidence for generation mechanisms of discrete and hiss-like whistler mode waves. *Geophysical Research Letters*, 41(14), 4805–4811. <https://doi.org/10.1002/2014gl060707>
- Hasegawa, A. (1969). Drift mirror instability in the magnetosphere. *Physics of Fluids*, 12, 2642–2650. <https://doi.org/10.1063/1.1692407>
- Jovanovic, D., & Simic, A. (2004). Electron-temperature-gradient instability of obliquely propagating whistlers. *Physica Scripta*, T113, 45–50. <https://doi.org/10.1238/Physica.Topical.113a00045>
- Kennel, C. F., & Petschek, H. E. (1966). Limit on stably trapped particle fluxes. *Journal of Geophysical Research*, 71(1), 1–28. <https://doi.org/10.1029/JZ071i001p00001>
- Le Contel, O., Leroy, P., Roux, A., Coillot, C., Alison, D., Bouabdellah, A., et al. (2016). The search-coil magnetometer for MMS. *Space Science Reviews*, 199(1–4), 257–282. <https://doi.org/10.1007/s11214-014-0096-9>
- Li, L., Omura, Y., Zhou, X.-Z., Zong, Q.-G., Rankin, R., Yue, C., et al. (2023). Chorus wave generation modulated by field line resonance and mirror-mode ULF waves. *Journal of Geophysical Research: Space Physics*, 128(2), e2022JA031127. <https://doi.org/10.1029/2022JA031127>
- Li, W., Mourenas, D., Artemyev, A. V., Bortnik, J., Thorne, R. M., Kletzing, C. A., et al. (2016). Unraveling the excitation mechanisms of highly oblique lower band chorus waves. *Geophysical Research Letters*, 43(17), 8867–8875. <https://doi.org/10.1002/2016GL070386>
- Li, W., Thorne, R. M., Bortnik, J., Nishimura, Y., & Angelopoulos, V. (2011). Modulation of whistler mode chorus waves: 1. Role of compressional PC4-5 pulsations. *Journal of Geophysical Research*, 116(A6), A06205. <https://doi.org/10.1029/2010JA016312>
- Li, W., Thorne, R. M., Bortnik, J., Tao, X., & Angelopoulos, V. (2012). Characteristics of hiss-like and discrete whistler mode emissions. *Geophysical Research Letters*, 39(18), L18106. <https://doi.org/10.1029/2012GL053206>
- Lindqvist, P.-A., Olsson, G., Torbert, R. B., King, B., Granoff, M., Rau, D., et al. (2016). The spin-plane double probe electric field instrument for MMS. *Space Science Reviews*, 199(1–4), 137–165. <https://doi.org/10.1007/s11214-014-0116-9>

- Lu, Q., Ke, Y., Wang, X., Liu, K., Gao, X., Chen, L., & Wang, S. (2019). Two-dimensional general curvilinear particle-in-cell (gcPIC) simulation of rising-tone chorus waves in a dipole magnetic field. *Journal of Geophysical Research: Space Physics*, 124(6), 4157–4167. <https://doi.org/10.1029/2019JA026586>
- Meredith, N. P., Horne, R. B., Thorne, R. M., Summers, D., & Anderson, R. R. (2004). Substorm dependence of plasmaspheric hiss. *Journal of Geophysical Research*, 109(A6), A06209. <https://doi.org/10.1029/2004JA010387>
- Miyoshi, Y., Morioka, A., Kataoka, R., Kasahara, Y., & Mukai, T. (2007). Evolution of the outer radiation belt during the November 1993 storms driven by corotating interaction regions. *Journal of Geophysical Research*, 112(A5), A05210. <https://doi.org/10.1029/2006JA012148>
- Miyoshi, Y., Morioka, A., Obara, T., Misawa, H., Nagai, T., & Kasahara, Y. (2003). Rebuilding process of the outer radiation belt during the November 3, 1993, magnetic storm—NOAA and EXOS-D observations. *Journal of Geophysical Research*, 108(A1), 1004. <https://doi.org/10.1029/2001JA007542>
- Mourenas, D., Artemyev, A., Agapitov, O., Krasnoselskikh, V., & Mozer, F. S. (2015). Very oblique whistler generation by low-energy electron streams. *Journal of Geophysical Research*, 120(5), 3665–3683. <https://doi.org/10.1002/2015JA021135>
- Pollock, C., Moore, T., Jacques, A., Burch, J., Gliese, U., Saito, Y., et al. (2016). Fast plasma investigation for magnetospheric multiscale. *Space Science Reviews*, 199(1), 331–406. <https://doi.org/10.1007/s11214-016-0245-4>
- Rae, I. J., Mann, I. R., Watt, C. E. J., Kistler, L. M., & Baumjohann, W. (2007). Equator-S observations of drift mirror mode waves in the dawnside magnetosphere. *Journal of Geophysical Research*, 112(A11), A11203. <https://doi.org/10.1029/2006JA012064>
- Russell, C. T., Anderson, B. J., Baumjohann, W., Bromund, K. R., Dearborn, D., Fischer, D., et al. (2016). The magnetospheric multiscale magnetometers. *Space Science Reviews*, 199(1–4), 189–256. <https://doi.org/10.1007/s11214-014-0057-3>
- Smith, E. J., & Tsurutani, B. T. (1976). Magnetosheath lion roars. *Journal of Geophysical Research*, 81(13), 2261–2266. <https://doi.org/10.1029/JA081i013p02261>
- Soto-Chavez, A. R., Lanzerotti, L. J., Manweiler, J. W., Gerrard, A., Cohen, R., Xia, Z., et al. (2019). Observational evidence of the drift-mirror plasma instability in Earth's inner magnetosphere. *Physics of Plasmas*, 26(4), 042110. <https://doi.org/10.1063/1.5083629>
- Thorne, R., & Tsurutani, B. (1981). The generation mechanism for magnetosheath lion roars. *Nature*, 293(5831), 384–386. <https://doi.org/10.1038/293384a0>
- Treumann, R. A., & Baumjohann, W. (2019). Mirror mode physics: The amplitude limit. *Annales Geophysicae*, 37(5), 971–988. <https://doi.org/10.5194/angeo-2019-86>
- Tsurutani, B. T., Lakhina, G. S., Verkhoglyadova, O. P., Echer, E., Guarnieri, F. L., Narita, Y., & Constantinescu, D. O. (2011). Magnetosheath and heliosheath mirror mode structures, interplanetary magnetic decreases, and linear magnetic decreases: Differences and distinguishing features. *Journal of Geophysical Research*, 116(A2), A02103. <https://doi.org/10.1029/2010JA015913>
- Tsurutani, B. T., & Smith, E. J. (1974). Postmidnight chorus: A substorm phenomenon. *Journal of Geophysical Research*, 79(1), 118–127. <https://doi.org/10.1029/Ja079i001p00118>
- Tsurutani, B. T., & Smith, E. J. (1977). Two types of magnetospheric ELF chorus and their substorm dependences. *Journal of Geophysical Research*, 82(32), 5112–5128. <https://doi.org/10.1029/JA082i032p05112>
- Tsurutani, B. T., Smith, E. J., Anderson, R. R., Ogilvie, K. W., Scudder, J. D., Baker, D. N., & Bame, S. J. (1982). Lion roars and nonoscillatory drift mirror waves in the magnetosheath. *Journal of Geophysical Research*, 87(A8), 6060–6072. <https://doi.org/10.1029/JA087iA08p06060>
- Xie, H. (2019). BO: A unified tool for plasma waves and instabilities analysis. *Computer Physics Communications*, 244, 343–371. <https://doi.org/10.1016/j.cpc.2019.06.014>
- Zhang, Y., Matsumoto, H., & Kojima, H. (1998). Lion roars in the magnetosheath: The Geotail observations. *Journal of Geophysical Research*, 103(A3), 4615–4626. <https://doi.org/10.1029/97JA02519>